Engineering Science and Technology, an International Journal 52 (2024) 101674

Contents lists available at ScienceDirect

Engineering Science and Technology, an International Journal

journal homepage: www.elsevier.com/locate/jestch

Rigorous design and experimental validation of non-reciprocal bandpass filter with ultrawide high reverse isolation bandwidth

Girdhari Chaudhary [a], Yongchae Jeong [b,*]

[a] JIANT-IT Human Resource Development Center, Division of Electronic and Information Engineering, Jeonbuk National University, Jeonju-si, Jeollabuk-do 54896, Republic of Korea
[b] Division of Electronic Engineering, Jeonbuk National University, Jeonju-si, Jeollabuk-do 54896, Republic of Korea

ARTICLE INFO

Keywords:
Isolator
Spatio temporal modulation
Non-reciprocal bandpass filter
Numerical design
Time-modulated resonators

ABSTRACT

This work presents a rigorous design and experimental validation of a non-reciprocal bandpass filter (NBPF) employing time-modulated resonators with progressive phase shift sinusoidal modulation signal to achieve low forward transmission insertion loss (IL) and ultrawide high reverse isolation bandwidth. Analytical design equations have been derived for numerical design of NBPF asl well as providing insights of nonreciprocal frequency response. Additionally, these proposed analytical spectral *S*-parameters offer the flexibility to design NBPFs with arbitrary termination port impedances. This work also demonstrates a systematic approach to find modulation parameters without relying on optimization methods. It has established empirical relationships between the modulation parameters and the filters specifications to achieve low forward transmission IL and reverse isolation exceeding 15 dB at entire frequency range. The accuracy of the proposed NBPF design has been confirmed by comparing with harmonic balance simulation results of microstrip line NBPF. For experimental validation, three prototypes of NBPF with different termination port impedances are designed, implemented, and manufactured. In experimental results, the frequency of NBPFs can be continously tuned from 1.62 GHz to 1.94 GHz (17.98 %) with maximum forward transmission IL ($|S_{21}|$) of 5.40 dB and input/output return loss higher than 12 dB. For each frequency tuning state, the reverse isolation ($|S_{12}|$) exceeds higher than 20 dB across the entire frequency range.

1. Introduction

Multi-functional non-reciprocal components are highly desirable for multi-functional RF front-end chains that can accommodate the emerging wireless applications. Integrating functions of bandpass filter, impedance matching, and isolator into single circuit is one emerging approach to facilitate the development of multi-functional miniaturized RF front-end chains. Non-reciprocal components (such as circulator and isolator) are fundamental elements of communication systems, radar, and instrumentation systems due to their ability to cancel self-interference between transmitting and receiving signals in full duplex (FD) systems and to protect their RF front-ends from unwanted reflections [1–5]. In the past, non-reciprocal components such as circulators and isolators have been designed by using ferrite magnetic materials. Nevertheless, these ferrites based non-reciprocal components suffer from being relatively large circuit size, costly, and lack of compatibility with integrated circuits [6–8]. To avoid the use of ferrite magnetic material, combination of linear and non-linear circuits have been employed to design non-reciprocal components, however, these approaches suffer from drawbacks such as poor noise figure, limited power handling, and small dynamic range [7–9]. Recent research efforts have focused on development of magnetless non-reciprocal circuits through three main techniques: a) exploiting inherent unilateral properties of transistors [10–14], b) breaking reciprocity through staggered commutation of N-path filters [15–17], and c) utilizing spatiotemporal modulation (STM) [18–20].

STM has been demonstrated as an alternative effective approach to achieve non-reciprocity without using any magnetic materials and has

* Corresponding author.
E-mail address: ycjeong@jbnu.ac.kr (Y. Jeong).

https://doi.org/10.1016/j.jestch.2024.101674
Received 24 October 2023; Received in revised form 28 February 2024; Accepted 9 March 2024

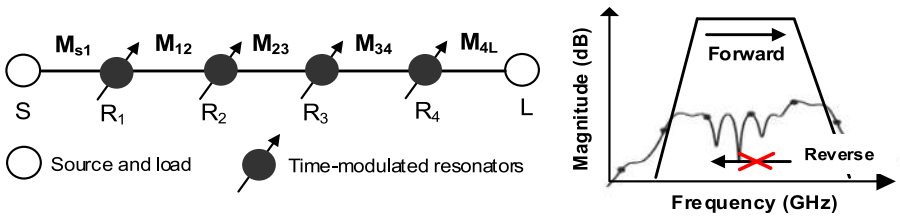

Fig. 1. Coupling diagram of the proposed non-reciprocal bandpass filter.

been widely employed in optical devices. In recent year, STM has been employed to design magnetless circulator [21,22], non-reciprocal bandpass filters (NBPFs) [23,24], and non-reciprocal filtering power divider [25,26]. Magnetless NBPF that allow transmission of signal in only direction ($|S_{21}| \neq |S_{12}|$) have been demonstrated either in the lumped-element or microstrip-type configurations by modulating resonators with progressive phase shift sinusoidal signal. In [23,24,27,28], NBPFs have been presented using a lumped element time-modulated resonator. In [29], NBPF is demonstrated using time-varying coupling matrix. In [30,31,32,33], microstrip line NBPFs have been implemented using half-wavelength and quarter wavelengths time modulated resonators. To achieve selective frequency characteristics, single-ended and differential NBPFs with a quasi-elliptic transfer function are implemented in subsequent works [34–36]. In most recently, coupling mixed static and time-modulated resonators has shown to be an effective approach for enhancing reverse isolation bandwidth of NBPF without increasing number of time-modulated resonators [37]. Despite significant research efforts, previously reported NBPFs may run into following limitations:

1) Narrow reserve isolation ($|S_{12}|$) bandwidth: The previously aforementioned NBPFs are able to achieve high reverse isolation solely at the center frequency(f_0). In [23,24,29,35], NBPFs are demonstrated where reverse isolation exhibits a single null characteristic, reaching value up to 40 dB only at center frequency. Similarly, NBPFs with two nulls reverse isolation characteristics have been achieved in [27,28,31,32,33]. However, the reverse isolation at center frequency is limited to 20 dB and the reverse isolation bandwidth of 20 dB is very narrow, confined to a range of 23 to 50 MHz.
2) The previously reported NBPFs in [23,31–34,36] have predominantly depended on parametric studies conducted through harmonic balance (HB) simulations for obtaining optimum modulation parameters that achieve the non-reciprocity. However, HB simulations can be time consuming due to convergence requirement of the HB algorithm.

Aiming to overcome these limitations of previously reported works, this paper presents a rigorous design to achieve NBPF response with ultra-wide reverse isolation. For achieving non-reciprocal response, analytical spectral *S*-parameters have been derived and the empirical relationships between modulation parameters and filter specifications have been established. These relationships enable optimization free modulation parameters for achieving NBPF response with minimal forward transmission IL and high isolation in reverse direction of transmission at all frequencies. The accuracy of the proposed design has been confirmed by comparing results with HB simulation results.

2. Design theory

2.1. Design method of the proposed non-reciprocal bandpass filter

Fig. 1 depicts the coupling diagram of the proposed non-magnetic

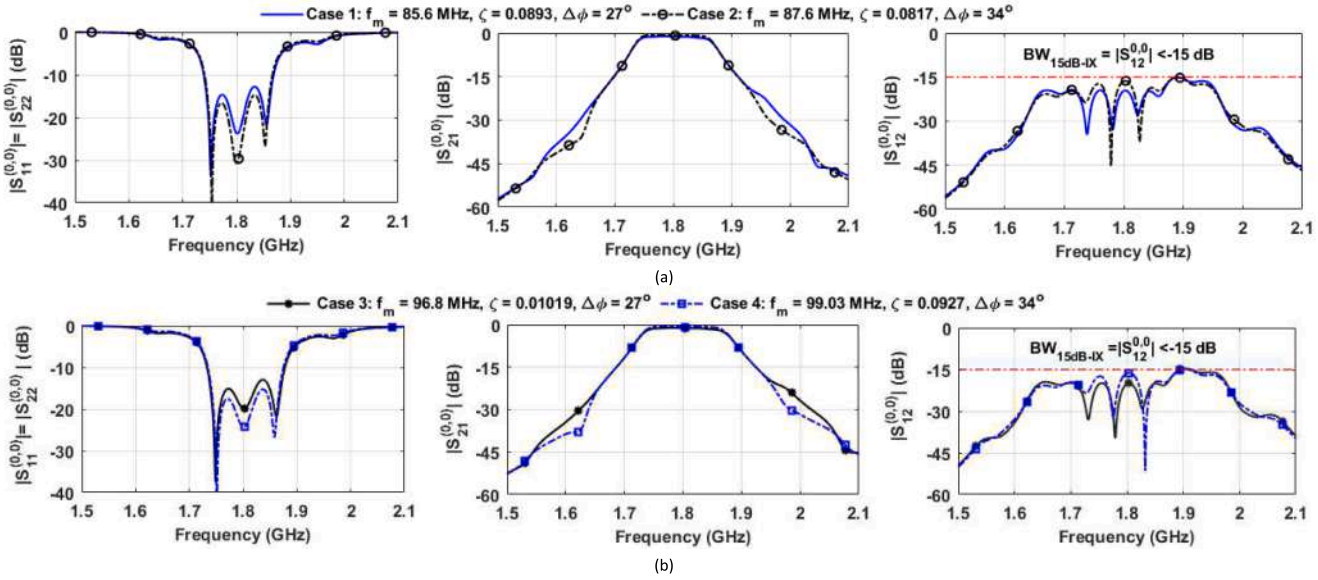

Fig. 2. Numerically calculated frequency responses of NBPF with BW = 100 MHz, N_{har} = 7 (i.e. k = -3,-2,-1,0, +1, +2, +3), and different LPF element values: (a) Chebyshev LPF element values with passband ripple of 0.0138 dB (in-band RL >25 dB at static state): $g_0 = 1$, $g_1 = 0.7533$, $g_2 = 1.2252$, $g_3 = 1.3712$, $g_4 = 0.6731$, $g_5 = 1.1192$, and (b) Chebyshev LPF element values with passband ripple of 0.0043 dB (in-band RL >30 dB at static state): $g_0 = 1$, $g_1 = 0.6209$, $g_2 = 1.1279$, $g_3 = 1.2016$, $g_4 = 0.5829$, $g_5 = 1.0653$.

Table 1
NBPF specifications and calculated frequency responses according to modulation parameters.

	Ripple (ε_r) for LPF prototype	Modulation parameters			IL = $\lvert S_{21}\rvert$ (dB)	$RL_{min} = \lvert S_{11}\rvert$ (dB)	Reverse isolation (IX) = $\lvert S_{12}\rvert$ within passband (dB)	IX bandwidth (MHz)	
		f_m (MHz)	m	$\triangle\varphi$				$BW_{20dB\text{-}IX}$	$BW_{15dB\text{-}IX}$
Case 1	0.0138 dB (RL_s = 25 dB)	85.7	0.0893	27°	<1	>12.85	>20	200	∞(AFR)
Case 2	BW = 100 MHz	87.7	0.0817	33°	<0.83	>14.80	>16.8	200	∞ (AFR)
Case 3	0.0043 dB (RL_s = 30 dB)	96.8	0.1019	27°	<1	>13.1	>20	230	∞ (AFR)
Case 4	BW = 100 MHz	99.1	0.0927	27°	<0.70	>15.2	>16.5	240	∞ (AFR)

$BW_{20dB\text{-}IX}$: bandwidth of reverse isolation (IX) when $|S_{12}|< -15$ dB, $BW_{15dB\text{-}IX}$: bandwidth of reverse isolation (IX) when $|S_{12}|< -15$ dB. AFR: entire RF frequency range.

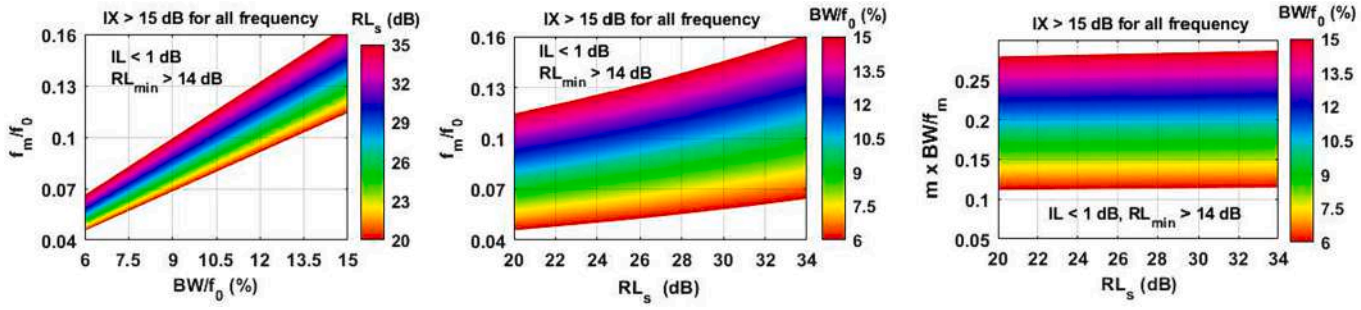

Fig. 3. Modulation parameters (f_m and m) of proposed NBPF according to bandwidth (BW) and in-band return loss (RLs) at static state (without modulation). These modulation parameters can achieve NBPF frequency response with forward transmission insertion loss (IL) < 1 dB and reverse isolation (IX) >15 for all frequency.

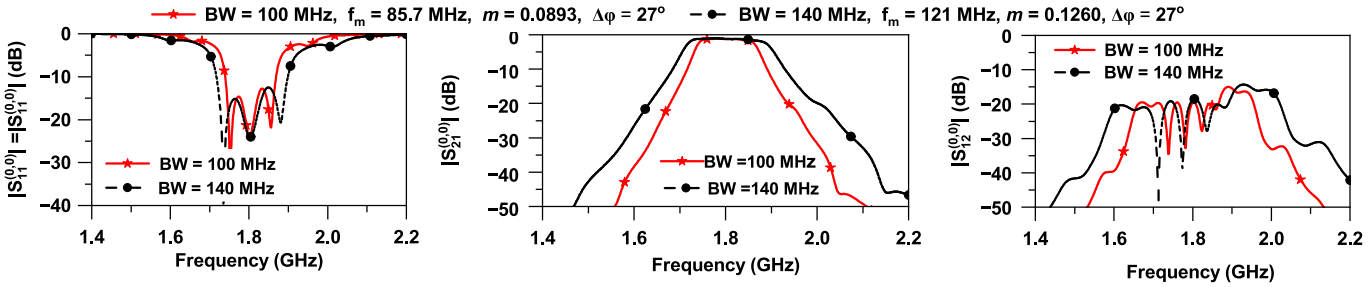

Fig. 4. Numerically calculated frequency response of proposed NBPF with different bandwidths. Other specifications: $z_s = z_L = 1\ \Omega$, $f_0 = 1.80$ GHz and low pass filter element values: $g_0 = 1$, $g_1 = 0.7533$, $g_2 = 1.2252$, $g_3 = 1.3712$, $g_4 = 0.6731$, $g_5 = 1.1192$.

non-reciprocal BPF where R_1, R_2, R_3, and R_4 represent time-modulated resonators and S and L denote source (RF port 1) and load (RF port 2), respectively. The source and load ports are terminated with arbitrary impedances z_s and z_L which are normalized to 50 Ω. Notably, source and load ports termination impedances comprise of normalized real part and frequency dependent complex part ($\omega L_{s,L}$or$1/\omega C_{s,L}$) where ω is an operating frequency in radian.

$$z_s = r_s \pm jx_s = \begin{cases} r_s + j\omega L_s \\ r_s - j/\omega C_s \end{cases}, z_L = r_L \pm jx_L = \begin{cases} r_L + j\omega L_L \\ r_L - j/\omega C_L \end{cases} \quad (1)$$

In (1), $r_{s,L}$ represent the real part of port 1 and 2 termination impedances. Similarly, $L_{s,L}$ and $C_{s,L}$ are normalized inductance and capacitance of port 1 and port 2 termination impedances. To achieve non-reciprocal BPF response, four resonators are modulated with time-varying capacitors C_i (t), as given below:

$$C(t) = C_0[1 + m\cos\{\omega_m t + (i-1)\Delta\varphi\}], i = 1, 2, 3, 4 \quad (2)$$

where $f_m = 2\pi\omega_m$, $\Delta\varphi$ and m are the modulation frequency, progressive phase shift of modulating waveform, and the modulation index, respectively [27]. Similarly, C_0 presents the nominal capacitance when modulation signal is not applied. Modulating resonators with progressive phase shift sinusoidal signal leads to generation of intermodulation (IM) products and as a result, RF input power is distributed among the IM products [23,28]. The non-reciprocity originated from the phase difference and magnitude of RF power distributed IM products in forward direction and reverse direction. In forward direction, RF power distributed among IM products is collected in a constructive manner at output port to achieve minimal transmission insertion loss (IL). Conversely, in reverse direction, it is collected in a destructive manner at outport port to achieve high reverse isolation.

$$\lambda_i = \begin{bmatrix} & & & & & & \\ & & & & & & \\ & & & & & & \\ \cdots & \frac{1}{2\pi BW}\left(\omega-2\omega_m-\frac{\omega_{0i}^2}{\omega-2\omega_m}\right) & \frac{m(\omega-2\omega_m)}{4\pi BW}e^{-j(i-1)\Delta\varphi} & 0 & 0 & 0 & \cdots \\ \cdots & \frac{m(\omega-\omega_m)}{4\pi BW}e^{j(i-1)\Delta\varphi} & \frac{1}{2\pi BW}\left(\omega-\omega_m-\frac{\omega_{0i}^2}{\omega-\omega_m}\right) & \frac{m(\omega-\omega_m)}{4\pi BW}e^{-j(i-1)\Delta\varphi} & 0 & 0 & \cdots \\ \cdots & 0 & \frac{m\omega}{4\pi BW}e^{j(i-1)\Delta\varphi} & \frac{1}{2\pi BW}\left(\omega-\frac{\omega_{0i}^2}{\omega}\right) & \frac{m\omega}{4\pi BW}e^{-j(i-1)\Delta\varphi} & 0 & \cdots \\ \cdots & 0 & 0 & \frac{m(\omega+\omega_m)}{4\pi BW}e^{j(i-1)\Delta\varphi} & \frac{1}{2\pi BW}\left(\omega+\omega_m-\frac{\omega_{0i}^2}{\omega+\omega_m}\right) & \frac{m(\omega+\omega_m)}{4\pi BW}e^{-j(i-1)\Delta\varphi} & \cdots \\ \cdots & 0 & 0 & 0 & \frac{m(\omega+2\omega_m)}{4\pi BW}e^{j(i-1)\Delta\varphi} & \frac{1}{2\pi BW}\left(\omega+2\omega_m-\frac{\omega_{0i}^2}{\omega+2\omega_m}\right) & \cdots \\ & & & & & & \end{bmatrix} \begin{matrix} \\ \\ \\ \vdots \\ -2 \\ -1 \\ 0 \\ +1 \\ +2 \\ \vdots \\ \\ \\ \\ \end{matrix} \quad (3)$$

$k_1 \cdots$ -2 -1 0 +1 +2 $\cdots$ indices

k_2

$$\boldsymbol{S}_{11}^{(k_1,k_2)} = \boldsymbol{S}_{22}^{(k_1,k_2)} = U - \frac{\frac{2\omega_{01}}{\omega_0}\mathrm{M}_{s1}^2\left(\frac{\omega_{04}z_l}{\omega_0 r_L}\mathrm{M}_{s1}^2\mathrm{M}_{23}^2 + j\frac{\omega_{04}}{\omega_0}\mathrm{M}_{12}^2\lambda_2 + j\mathrm{M}_{23}^2\lambda_4 - \frac{\omega_{04}z_l}{\omega_0 r_L}\mathrm{M}_{s1}^2\lambda_2\lambda_3 - j\lambda_2\lambda_3\lambda_4\right)}{\left\{\begin{array}{l} \frac{\omega_{01}\omega_{04}}{\omega_0^2}\mathrm{M}_{12}^4 + \frac{\omega_{01}\omega_{04}z_sz_l}{\omega_0^2 r_s r_L}\mathrm{M}_{s1}^4\mathrm{M}_{23}^2 + j\mathrm{M}_{s1}^2\mathrm{M}_{23}^2\left(\frac{\omega_{04}z_L}{\omega_0 r_L}\lambda_1 + \frac{\omega_{01}z_s}{\omega_0 r_s}\lambda_4\right) - j\mathrm{M}_{s1}^2\left(\frac{\omega_{01}z_s}{\omega_0 r_s}\lambda_2\lambda_3\lambda_4 + \frac{\omega_{04}z_L}{\omega_0 r_L}\lambda_1\lambda_2\lambda_3\right) \\ +j\frac{\omega_{01}\omega_{04}}{\omega_0^2}\mathrm{M}_{s1}^2\mathrm{M}_{12}^2\left(\frac{z_s}{r_s}\lambda_2 + \frac{z_L}{r_L}\lambda_3\right) - \mathrm{M}_{23}^2\lambda_1\lambda_4 - \mathrm{M}_{12}^2\left(\frac{\omega_{04}}{\omega_0}\lambda_1\lambda_2 + \frac{\omega_{01}}{\omega_0}\lambda_3\lambda_4\right) - \frac{\omega_{01}\omega_{04}z_sz_l}{\omega_0^2 r_s r_L}\mathrm{M}_{s1}^4\lambda_2\lambda_3 + \lambda_1\lambda_2\lambda_3\lambda_4 \end{array}\right\}} \quad (4a)$$

$$\boldsymbol{S}_{21}^{(k_1,k_2)} = \frac{2\omega_{01}\omega_{04}\mathrm{M}_{s1}^2\mathrm{M}_{12}^2\mathrm{M}_{23}}{\omega_0^2\left\{\begin{array}{l} \frac{\omega_{01}\omega_{04}}{\omega_0^2}\mathrm{M}_{12}^4 + \frac{\omega_{01}\omega_{04}z_sz_l}{\omega_0^2 r_s r_L}\mathrm{M}_{s1}^4\mathrm{M}_{23}^2 + j\mathrm{M}_{s1}^2\mathrm{M}_{23}^2\left(\frac{\omega_{04}z_L}{\omega_0 r_L}\lambda_1 + \frac{\omega_{01}z_s}{\omega_0 r_s}\lambda_4\right) - j\mathrm{M}_{s1}^2\left(\frac{\omega_{01}z_s}{\omega_0 r_s}\lambda_2\lambda_3\lambda_4 + \frac{\omega_{04}z_L}{\omega_0 r_L}\lambda_1\lambda_2\lambda_3\right) \\ +j\frac{\omega_{01}\omega_{04}}{\omega_0^2}\mathrm{M}_{s1}^2\mathrm{M}_{12}^2\left(\frac{z_s}{r_s}\lambda_2 + \frac{z_L}{r_L}\lambda_3\right) - \mathrm{M}_{23}^2\lambda_1\lambda_4 - \mathrm{M}_{12}^2\left(\frac{\omega_{04}}{\omega_0}\lambda_1\lambda_2 + \frac{\omega_{01}}{\omega_0}\lambda_3\lambda_4\right) - \frac{\omega_{01}\omega_{04}z_sz_l}{\omega_0^2 r_s r_L}\mathrm{M}_{s1}^4\lambda_2\lambda_3 + \lambda_1\lambda_2\lambda_3\lambda_4 \end{array}\right\}} \quad (4b)$$

$$\boldsymbol{S}_{12}^{(k_1,k_2)} = \frac{2\omega_{01}\omega_{04}\mathrm{M}_{s1}^2\mathrm{M}_{12}^2\mathrm{M}_{23}}{\omega_0^2\left\{\begin{array}{l} \frac{\omega_{01}\omega_{04}}{\omega_0^2}\mathrm{M}_{12}^4 + \frac{\omega_{01}\omega_{04}z_sz_l}{\omega_0^2 r_s r_L}\mathrm{M}_{s1}^4\mathrm{M}_{23}^2 + j\mathrm{M}_{s1}^2\mathrm{M}_{23}^2\left(\frac{\omega_{04}z_L}{\omega_0 r_L}\lambda_1 + \frac{\omega_{01}z_s}{\omega_0 r_s}\lambda_4\right) - j\mathrm{M}_{s1}^2\left(\frac{\omega_{01}z_s}{\omega_0 r_s}\lambda_4\lambda_3\lambda_2 + \frac{\omega_{04}z_L}{\omega_0 r_L}\lambda_3\lambda_2\lambda_1\right) \\ +j\frac{\omega_{01}\omega_{04}}{\omega_0^2}\mathrm{M}_{s1}^2\mathrm{M}_{12}^2\left(\frac{z_s}{r_s}\lambda_2 + \frac{z_L}{r_L}\lambda_3\right) - \mathrm{M}_{23}^2\lambda_4\lambda_1 - \mathrm{M}_{12}^2\left(\frac{\omega_{04}}{\omega_0}\lambda_2\lambda_1 + \frac{\omega_{01}}{\omega_0}\lambda_4\lambda_3\right) - \frac{\omega_{01}\omega_{04}z_sz_l}{\omega_0^2 r_s r_L}\mathrm{M}_{s1}^4\lambda_3\lambda_2 + \lambda_4\lambda_3\lambda_2\lambda_1 \end{array}\right\}} \quad (4c)$$

When RF signal frequency is applied to time-modulated resonators, various intermodulation products ($\omega + k\omega_m$) are generated [27,29]. Considering number of harmonics N_{har} (i.e. $k = \cdots$,-2,-1,0,+1,+2, $\cdots$), frequency-domain the spectral admittance matrix of the time-modulated resonators can be derived as (3) . While analyzing the interaction between different time-modulated resonators, couplings between resonators of the same harmonic order are only considered and these coupling coefficients retain the same values as in the absence of modulation [29]. As a result, the coupling element can be extracted using either Chebyshev or Butterworth filter prototype elements [38]. By employing spectral admittance, the spectral *S*-parameter of the proposed non-reciprocal BPF can be obtained as depicted in (4), where coupling matrix values are given as (5).

$$\mathbf{M}_{s1} = \mathbf{M}_{4L} = U/\sqrt{g_0 g_1} = U/\sqrt{g_4 g_5} \quad (5a)$$

$$\mathbf{M}_{12} = \mathbf{M}_{34} = U/\sqrt{g_1 g_2} = U/\sqrt{g_3 g_4} \quad (5b)$$

$$\mathbf{M}_{23} = U/\sqrt{g_2 g_3} \quad (5c)$$

where g_i is low-pass filter prototype element value [36] and U is unitary matrix of size $N_{har} \times N_{har}$. Ports 1 and 2 impedances are expanded at harmonic frequency $\omega + k_i\omega_m$, so that the spectral *S*-parameters of the proposed non-reciprocal BPF is $N_{har} \times N_{har}$ matrix. The *S*-

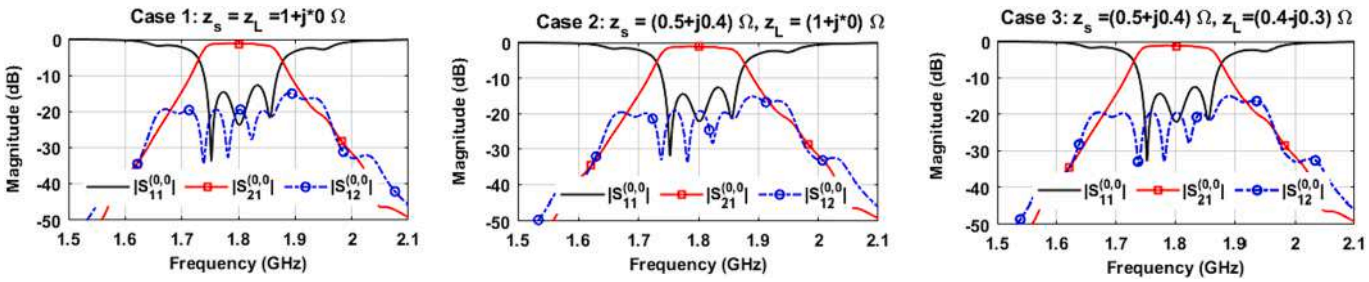

Fig. 5. Numerically calculated frequency response of the proposed NBPF with termination impedances. Other specifications: $f_0 = 1.80$ GHz, BW = 100 MHz, and low pass filter element values: $g_0 = 1$, $g_1 = 0.7533$, $g_2 = 1.2252$, $g_3 = 1.3712$, $g_4 = 0.6731$, $g_5 = 1.1192$. Modulation frequency: $f_m = 85.70$ MHz, $m = 0.090$ and $\triangle\varphi = 27°$.

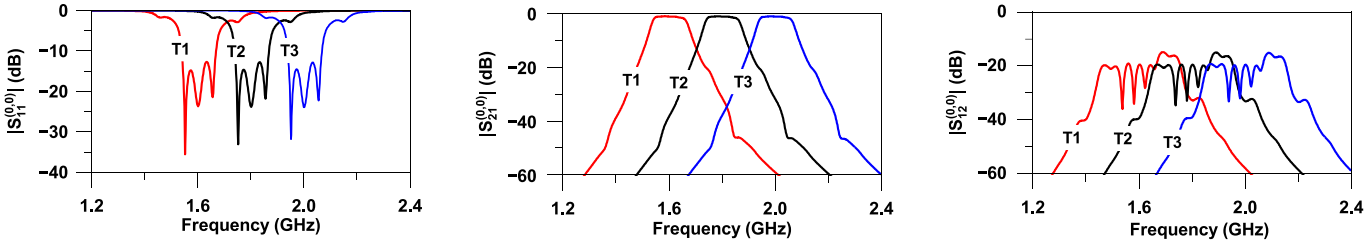

Fig. 6. Numerically calculated frequency response of proposed NBPF with tunable center frequency: Other parameters: $z_s = z_L = 1\ \Omega$, $f_0 = 1.6$–2 GHz, BW = 100 MHz, and low pass filter element values $g_0 = 1$, $g_1 = 0.7533$, $g_2 = 1.2252$, $g_3 = 1.3712$, $g_4 = 0.6731$, $g_5 = 1.1192$. Modulation parameters: $f_m = 85.70$ MHz, $m = 0.090$ and $\triangle\varphi = 27°$.

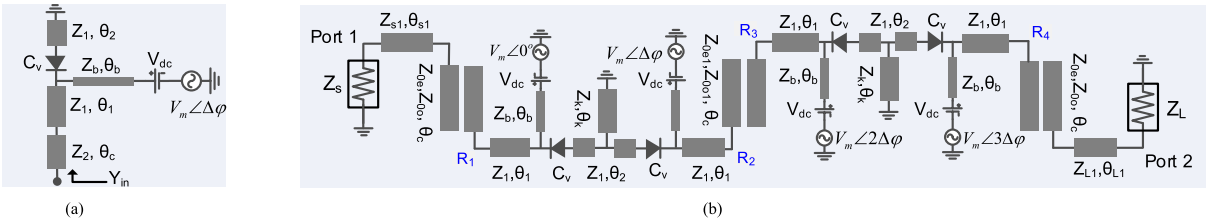

Fig. 7. Microstrip line implementation of the proposed NBPF: (a) time-modulated transmission line resonator and (b) overall circuit of transmission line NBPF.

parameter $S_{21}^{(k_1,k_2)}$ signifies the power transfer from the frequency component $\omega + k_1\omega_m$ at port 1 to frequency component $\omega + k_2\omega_m$ at port 2. For instance, $S_{21}^{(0,0)} = S_{21}$ symbolizes the power transfer from port 1 at fundament frequency to port 2 at fundamental frequency, involving multiple transmission paths.

To match arbitrary termination complex impedances of port 1 and 2, the resonant frequencies of the first and last time-modulated resonator should be detuned from original resonant frequency ω_0 according to (6).

$$\omega_{01,4} = \begin{cases} \omega_0\left\{\sqrt{1+\left(\frac{\omega_o L_{s,L}\Delta}{2r_s g_0 g_1}\right)^2} + \frac{\omega_o L_{s,L}\Delta}{2r_s g_0 g_1}\right\} \\ \omega_0\left\{\sqrt{1+\left(\frac{\Delta}{2r_s g_0 g_1 \omega_o C_{s,L}}\right)^2} - \frac{\Delta}{2r_s g_0 g_1 \omega_o C_{s,L}}\right\} \end{cases} \quad (6)$$

where $\triangle = \mathrm{BW}/f_0$ and BW is bandwidth of filer at static state (without modulation). In addition, the couplings value between source/load and first/last resonators should be modified as $M'_{s1} = M_{s1}/\sqrt{r_s}$ and $M'_{4L} = M_{4L}/\sqrt{r_L}$ depending on real part impedance of port 1 and 2, respectively. If the imaginary parts of z_s and z_L are zero, the resonant frequencies of all resonators remain same as original resonant frequency ω_0.

Based on (4), NBPF with $f_0 = 1.80$ GHz and BW = 100 MHz is numerically simulated using different coupling matrices. The coupling matrices are extracted using Chebyshev LPF with in-band return loss (RL) of better than 25 dB and 30 dB in static state, respectively. The numerically calculated frequency responses of NBPFs are shown in Fig. 2. The NBPF frequency responses corresponding modulation parameters (f_m, m, $\Delta\varphi$) are summarized in Table 1. As observed from these results, non-reciprocal response ($|S_{21}| \neq |S_{12}|$) is achieved when resonators are modulated with progressive phase shift modulation signal. The numerically calculated results shows that the proposed NBPF exhibits the forward transmission IL (IL= $|S_{21}|$) < 1.20 dB, input/output port return loss ($|S_{11}| = |S_{22}|$) >14 dB within passband, and reverse isolation (IX = $|S_{12}|$) >15 dB for entire RF frequency range. Since the network is lossless, the IL in forward direction is due to power that is converted to IM products and is not entirely converted back to the fundamental frequency. Notably, the 15 dB reverse IX bandwidth ($\mathrm{BW}_{15\mathrm{dB\text{-}IX}}$) of the proposed NBPF is infinite. In addition, the modulation frequency f_m increases as the passband ripple of LPF decreases. Similarly, high reverse IX within wide bandwidth is achieved when progressive phase shift is low such as $\Delta\varphi = 27°$. The reverse IX is higher than 20 dB within entire passband (20-dB IX bandwidth >200 MHz) when $f_m = 85.7$ MHz, $m = 0.0893$, $\Delta\varphi = 27°$ in case of LPF with ripple of 0.0138 dB (i.e., in-band RL >25 dB at static state) and $f_m = 96.8$ MHz, $m = 0.1019$, $\Delta\varphi = 27°$ in case of LPF with ripple of 0.0043 dB (*i.e.*, in-band RL >30 dB at static state).

Based on these numerical simulation results, the interesting empirical relationships between modulation parameters and filter specifications can be derived as (7) and (8).

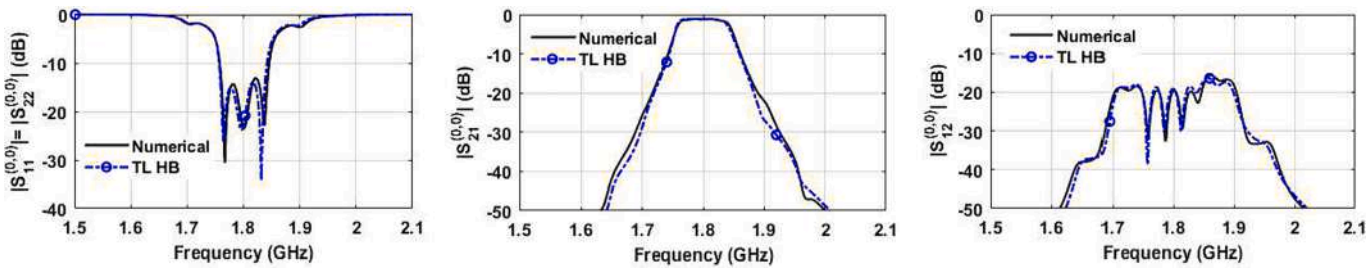

Fig. 8. Comparison results between numerical simulation and transmission line (TL) harmonic balance (HB) simulation. TL parameters: $Z_{s1} = Z_{L1} = Z_1 = Z_k = 70\ \Omega$, $\theta_{s1} = \theta_{L1} = 45.3^\circ$, $Z_{0e} = 93.76\ \Omega$, $Z_{0o} = 44.17\ \Omega$, $\theta_c = 25^\circ$, $\theta_1 = 40^\circ$, $\theta_2 = 14^\circ$, $\theta_k = 2.04^\circ$, $Z_{0e1} = 64.15\ \Omega$, $Z_{0o1} = 56.83\ \Omega$, $Z_b = 110\ \Omega$, $\theta_b = 54^\circ$. Modulation parameters: $f_m = 56$ MHz, $\triangle\varphi = 30^\circ$, $V_m = 0.44$ V. Varactor diode SMV 1233-079LF from Skyworks. Electrical lengths of TLs are calculated at 1.5 GHz.

$$f_m = \left(0.3235\varepsilon_r^{-0.1466} + 0.2503\right) \times BW \tag{7a}$$

$$m = 1.81\varepsilon_r^{-0.008283} \times f_m/f_0 \tag{7b}$$

$$\Delta\varphi = 27^0 \tag{7c}$$

where

$$\varepsilon_r = -10\log_{10}\left(1 - 10^{-RL_s(dB)/10}\right) \tag{8}$$

and RL_s and BW are in-band return loss and bandwidth of filter at static state (without modulation), respectively.

As shown in (7) and (8), the modulation frequency f_m depends on BW and passband ripple (ε_r) of static filter (without modulation) whereas modulation index m depends on passband ripple ε_r, f_0, and f_m. Notably, equations (7) and (8) provide modulation parameters that enable the design of a NBPF with low forward IL < 1 dB, very high level of reverse IX over wide bandwidth (IX >15 dB for all frequency), and excellent impedance matching (RL_{min} >14 dB) within passband. Furthermore, these empirical relations offer a straightforward selection of modulation parameters without need of optimization that can be directly used in experimental verification of fabricated protype of NBPF.

Based on (7) and (8), Fig. 3 depicts the calculated modulation parameters according to filter specifications of static filter such as passband ripple (RL_{static}), bandwidth (BW), and center frequency (f_0). The BW and modulation frequency f_m are normalized to f_0 so that NBPF can be designed at any arbitrary center frequency f_0. As observed from Fig. 3, the modulation frequency (f_m) and modulation index (m) increase as BW and passband return loss (RL_s) of static filter increase.

To demonstrate the flexibity of design equations discussed previously, numerical simulations have been carried out and results are shown in Figs. 4 – 6. In these numerical results, modulation parameters are calculated using (7) and (8). Fig. 4 illustrates numerical simulation results with different BWs. As observed from Figures, the modulation frequency f_m and modulation index (m) increase as the BW increases.

Fig. 5 demonstrates the numerical results of the proposed NBPFs with different termination impedances. The numerical S-parameters results confirm that the NBPF response remains identical for any arbitrary input and output termination impedances of filter. These results demonstrated that the proposed analytical design equations are suitable for any arbitrarily terminated NBPF that exhibits low forward transmission IL, good matching, and high reverse IX with multiple nulls (IX >20 dB within passband and IX >15 dB for entire frequency range).

Fig. 6 depicts the numerically calculated frequency response, illustrating the frequency tunability features. The frequency tunable response of the proposed NBPF can be achieved by adjusting resonant frequencies of time-modulated resonators. As shown in Fig. 6, NBPF center frequency is adjusted continously from 1.60 GHz to 2 GHz while maintaining forward transmission IL <1 dB, input/output return losses >14 dB, and reverse isolation >15 dB for infinite frequency range in all tuning state.

2.2. Microstrip line implementation of the proposed non-reciprocal bandpass filter

Fig. 7(a) shows microstrip line implementation of quarter wavelength time-modulated resonator. Time-varying capacitors are implemented by reverse bias voltage varactor diodes. The time modulated resonator consists of transmission line (TL) sections with characteristics impedances of Z_2, Z_1, Z_b and electrical lengths of θ_c, θ_1, θ_2, θ_b and varactor diode with capacitance of C_v at specific reverse bias voltage. A modulation voltage V_m is provided to each varactor with a constant phase shift $\triangle\varphi$. The modulation signal is applied to varactor diode through TL with characteristics impedance of Z_b and electrical length of θ_b. Using Fig. 7(a), input admittance of time-modulated resonator can be found as (9).

$$Y_{in} = jY_2\frac{A_2 + jY_2\tan\theta_c}{Y_2 - A_2\tan\theta_c} \tag{9}$$

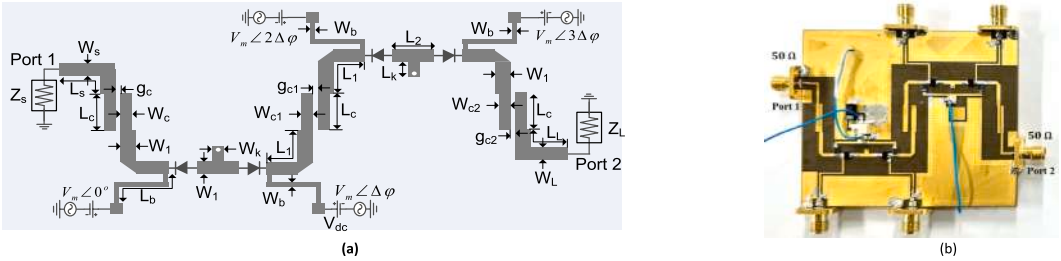

Fig. 9. (a) Physical dimensions and (b) photograph of fabricated Filter A: 50-to-50 Ω. Filter A dimensions: $W_s = W_L = 0.9$, $L_s = L_L = 12.2$, $W_c = W_{c2} = 1.05$, $L_c = 10.76$, $g_c = g_{c2} = 0.13$, $W_1 = 1.36$, $L_1 = 16$, $L_2 = 11.94$, $W_k = 1.40$, $L_k = 1.52$, $W_{c1} = 1.71$, $g_{c1} = 1.14$, $W_b = 0.6$, $L_b = 24$. Filter B dimensions: $W_s = 1.85$, $L_s = 14.2$, $W_c = 1.05$, $L_c = 10.76$, $g_c = 0.14$, $W_1 = 1.36$, $L_1 = 16$, $L_2 = 11.94$, $W_k = 1.40$, $L_k = 1.52$, $W_{c1} = 1.71$, $g_{c1} = 1.14$, $W_{c2} = 1.05$, $g_{c2} = 0.13$, $W_b = 0.6$, $L_b = 24$, $W_L = 0.9$, $L_L = 12.20$. Filter C dimensions: $W_s = 1.9$, $L_s = 14.2$, $W_c = 1.05$, $L_c = 10.76$, $g_c = 0.14$, $W_1 = 1.36$, $L_1 = 16$, $L_2 = 11.94$, $W_k = 1.40$, $L_k = 1.52$, $W_{c1} = 1.71$, $g_{c1} = 1.14$, $W_{c2} = 1.05$, $g_{c2} = 0.13$, $W_b = 0.6$, $L_b = 24$, $W_L = 0.7$, $L_L = 13.40$. Physical dimensions unit: millimeter (mm). Varactor diode: SMV 1233-079LF.

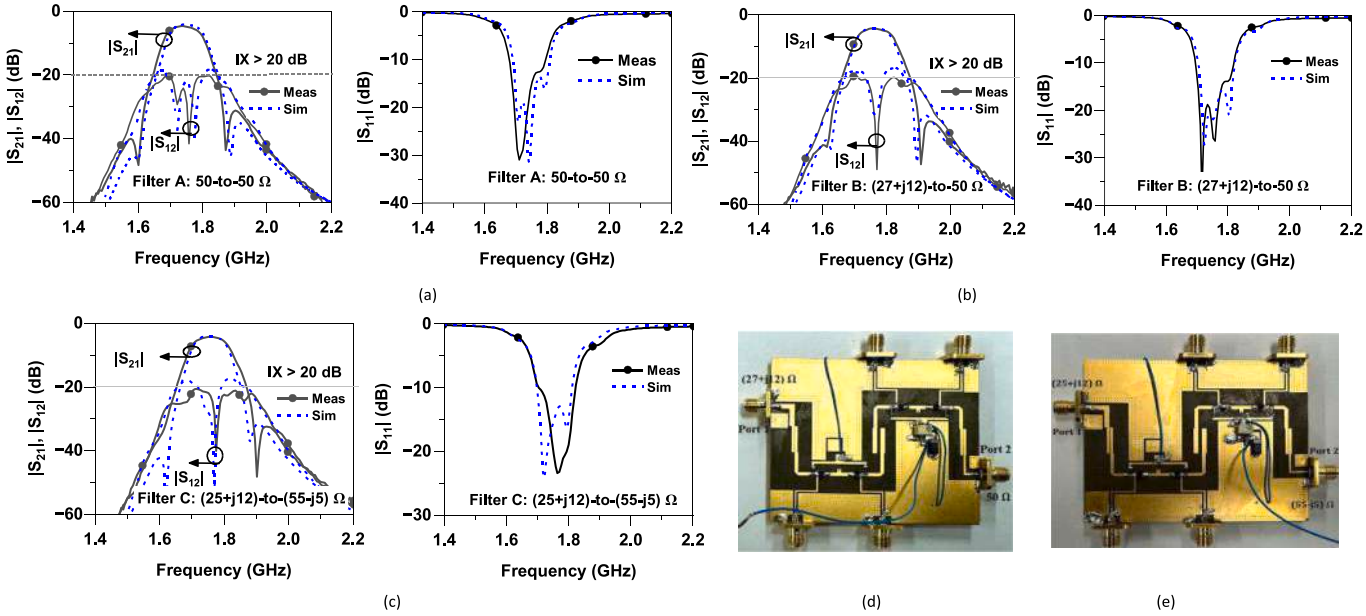

Fig. 10. Simulated and measured frequency response of NBPFs: (a) Filter A: 50-to-50 Ω NBPF, (b) Filter B: (27 + j12)-to-50 Ω, (c) Filter C: (25 + j12)-to-(55-j5) Ω NBPF, (d) photograph of fabricated Filter B, and (e) photograph of fabricated Filter C. Dashed lines: simulation results and solid lines: measurement results.

Table 2
Summary of measurement results of the proposed non-reciprocal bandpass filters.

		Filter A: 50-to-50 Ω			Filter B: (27 + j12)-to-50 Ω			Filter C: (25 + j12)-to-(55-j5) Ω		
		T1	T2	T3	T1	T2	T3	T1	T2	T3
Modulation parameters	f_m (MHz)	75	82	88	75	82	88	75	82	88
	V_m (V)	1.25	1.28	1.43	1.30	1.28	1.43	1.29	1.35	1.42
	$\triangle\varphi$ (Deg)	33°	34°	36°	33°	34°	36°	33°	34°	36°
Measured results	V_{dc} (V)	0	3.8	5.20	0	3.8	5.20	0	3.8	5.20
	f_0 (GHz)	1.62	1.74	1.94	1.62	1.76	1.94	1.62	1.76	1.92
	RL_{min} (dB)	>12	>13.4	>14.52	>11.20	>12.60	>11.50	>13.31	>16.08	>14.52
	IL (dB)	<5.40	<4.72	<4.30	<5.46	<4.35	<4.32	<5.58	<4.83	<4.47
	IX @ f_0 (dB)	22.89	24.24	22.90	20.44	33.87	22.07	20.30	30.50	31.25
	IX @ all frequeency (dB)	>20.5	>20	>18	>20.10	>20.10	>16.40	>19.10	>20.6	>17.50
	BW_{3dB} (MHz)	106	112	124	109	114	124	110	116	126
	$BW_{16dB\text{-}IX}$ (MHz)	∞	∞	∞	∞	∞	∞	∞	∞	∞
	Frequency tunability range (FTR)	1620–1940 (320 MHz): 17.98 % or 1:1.197			1620–1940 (320 MHz): 17.98 % or 1:1.197			1620–1920 (300 MHz): 16.94 % or 1:1.185		

IL: Maximum insertion loss within passband band, RL_{min}: Minimum input/output return loss within passband.
IX@f_0: Reverse isolation at cetner frequency (f_0), BW_{3dB}: 3-dB bandwidth of forward transmisison, $BW_{16dB\text{-}IX}$: 16-dB reverse isolation bandwidth.

where

$$A_2 = Y_1\frac{A_1 + Y_1\tan\theta_1}{Y_1 - A_1\tan\theta_1}, A_1 = \frac{Y_1\omega C_v\cot\theta_2}{Y_1\cot\theta_2 - \omega C_v} - Y_b\cot\theta_b \tag{10a}$$

$$Y_1 = \frac{1}{Z_1}, Y_2 = \frac{1}{Z_2}, Y_b = \frac{1}{Z_b} \tag{10b}$$

Resonant frequency of the resonator can be obtained by setting $im(Y_{in}) = 0$. The desired resonant frequency is obtained by controlling Z_1, Z_2, Z_b, θ_c, θ_1, θ_2, θ_b and varactor diode capacitance C_v.

Fig. 7(b) shows overall microstrip line implementation of the proposed NBPF, which consists of four quarter-wavelength TL time-modulated resonators. Time varying capacitors are implemented by modulating reverse bias voltage varactor diode (C_v). The coupling $\boldsymbol{M_{s1}}$ between port 1 and first resonator R_1 is implemented through series TL (Z_{s1}, θ_{s1}) and coupled line (Z_{0e}/Z_{0o}, θ_c). The coupling $\mathbf{M}_{12}$ as well as $\mathbf{M}_{34}$ between resonators R_1 and R_2 and resonators R_3 and R_4 are implemented using short-circuited stub (Z_k, θ_k). Likewise, the coupling $\mathbf{M}_{23}$ between resonators R_2 and R_3 is implemented with coupled line (Z_{0e1}/Z_{0o1}, θ_c). The sinusoidal modulation signals are applied through TL with characteristics impedance Z_b and electrical length θ_b. By adjusting these parameters, it is possible to achieve a high degree of isolation between the RF port and modulation signal source. Finally, coupling $\mathbf{M}_{L4}$ between last resonator R_4 and port 2 is implemented with coupled line (Z_{0e}/Z_{0o}, θ_c) and series TL (Z_{L1}, θ_{L1}). Based on discussion, the design procedure of microstrip line NBPF can be summarized as follows:

(a) Begin by selecting filter specifications including source/load termination impedances (Z_s/Z_L), center frequency (f_0), passband return loss (RL_s), and bandwidth (BW) at static state. Then, extract coupling matrix using (5) and modulation parameters (f_m, m, $\triangle\varphi$) using (7).
(b) Calculate desired coupling coefficients and external source/load quality factors (Q-factors) using $k_{i,i+1}^{des} = BW/f_0 \times M_{i,i+1}, i = 1, 2, 3$ and $Q_{es,L}^{des} = f_0/(BW \times M_{s1,4L})$.
(c) For microstrip line implementation of NBPF, select appropriate circuit parameters of time-modulated resonator using (9) to

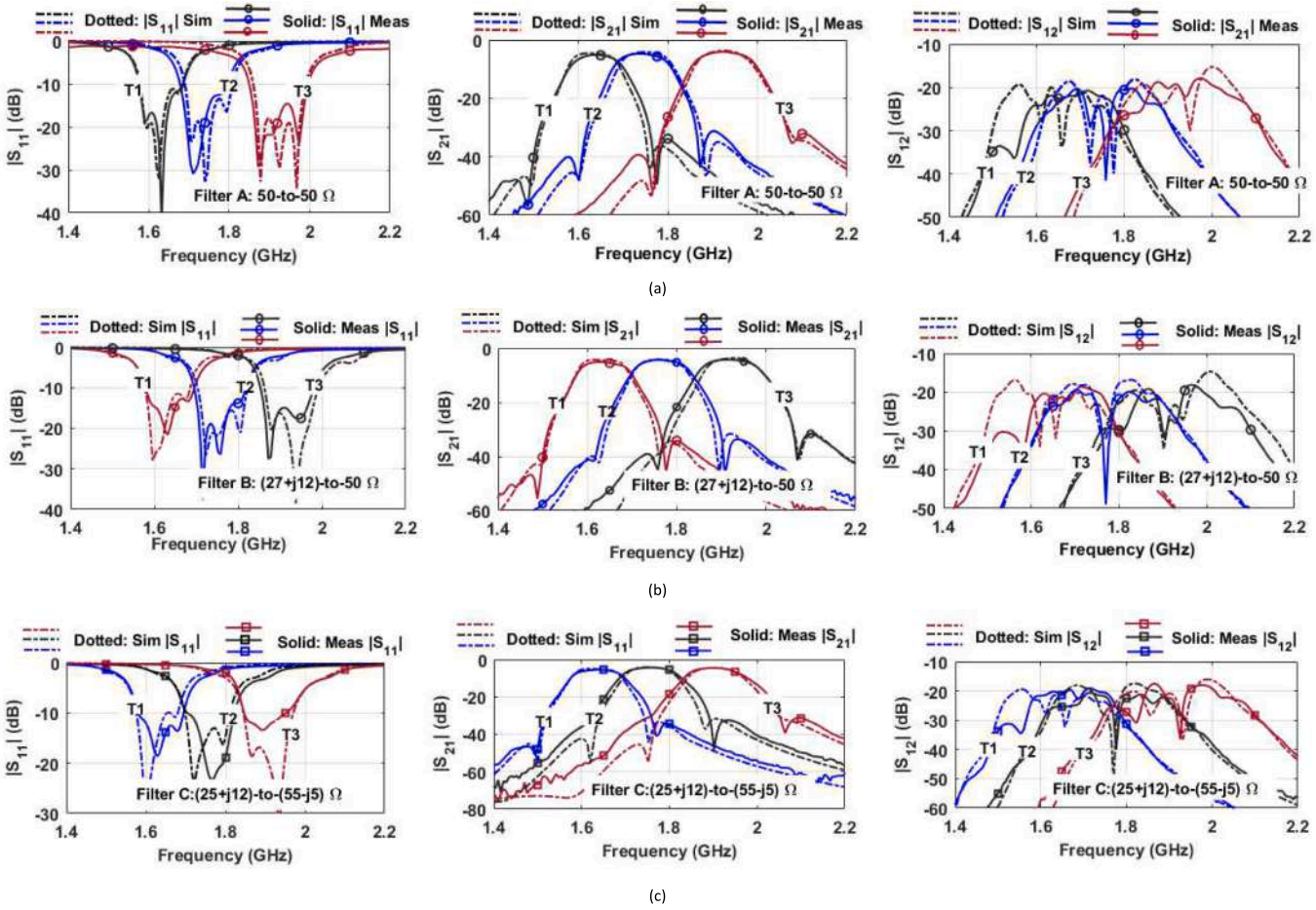

Fig. 11. Simulated and measured frequency tunability responses of NBPFs: (a) Filter A: 50-to-50 Ω NBPF, (b) Filter B: (27 + j12)-to-50 Ω, and (c) Filter C: (25 + j12)-to-(55-j5) Ω NBPF. Dashed line: simulation and solid lines: measurement.

achieve desired passband frequency. Likewise, extract coupling coefficients using $k_{i,i+1} = \left(f_h^2 - f_l^2\right)/\left(f_h^2 + f_l^2\right), i = 1, 2, 3$ where f_h and f_l are higher and lower frequency peaks appeared in $|S_{21}|$ of two coupled resonators, respectively [38]. The desired coupling coefficient between resonator R_1 and R_2 as well as between resonators R_3 and R_4 can be extracted by controlling Z_k and θ_k. Similarly, the desired coupling coefficient between resonators R_2 and R_3 can be obtained by controlling Z_{0e1} and Z_{0o1}.

(d) The external Q-factor can be determined using $Q_{eS,L}^{ext} = \omega_0 \tau_{s11}(\omega_0)/4$, where $\tau_{s11}(\omega_0)$ is group delay of S_{11} at resonant angular frequency ω_0 [38]. The coupling between input/output port and resonator R_1/R_4 is achieved through series TL (Z_{s1}, θ_{s1}) and coupled line (Z_{0e}/Z_{0o}, θ_c). The desired external Q-factors can be extracted by controlling Z_{s1}, θ_{s1} Z_{0e}/Z_{0o}, and θ_c.

(e) Optimize physical dimensions of microstrip line NBPF using co-simulation between ANYSYS HFSS and Keysight Advanced Design System (ADS) harmonic balance (HB) simulator to achieve desired non-reciprocal filter response.

To demonstrate accuracy of the proposed design, the numerically calculated S-parameters results of NBPF are compared with microstrip line NBPF and results are shown in Fig. 8. The frequency response of microstrip line NBPF are obtained using Keysight ADS with HB module. For HB simulation, we employed the SPICE equivalent circuit model of varactor SMV 1233-079LF, as provided by manufacturer [39]. The circuit parameters and modulation parameters of microstrip line NBPF are depicted in Fig. 8. For numerical calculation, the center frequency and bandwidth are specified as $f_0 = 1.8$ GHz and BW = 68 MHz. The coupling matrix is extracted using LPF prototype with passband ripple of 0.0138 dB (i.e. $RL_s = 25$ dB at static state). For the given filter specifications, the modulation parameters are calculated using (7) and (8) and given as $f_m = 57.90$ MHz, $m = 0.0598$, $\triangle\varphi = 27^\circ$. As shown in Fig. 8, the numerically calculated S-parameters are well agreed with S-parameters of the microstrip line NBPF obtained through HB simulation. The proposed microstrip line NBPF exhibits good input/output matching with three pole RL >14 within passband. The forward transmission IL is less than 1 dB and IX is higher than 20 dB within passband and IX is higher than 15.5 dB for all frequency range. These results confirmed that the proposed numerical design of NBPF enables a straightforward selection of modulation parameters without need of optimization that can directly be used prototyping and verification of microstrip line NBPF with low forward IL and high IX over wide bandwidth (IX >15 dB for entire frequency range).

3. Experimental results

For proof of concept, three prototypes of microstrip line NBPFs with different termination impedances (Filter A: 50-to-50 Ω, Filter B: (27 + j12)-to-50 Ω and Filter C: (25 + j12)-to-(55-j5) Ω) are designed and manufactured on RT/duroid 5880 substrate with a dielectric constant of 2.2 and thickness of 0.78 mm. The NBPFs are designed to have BW of 100 MHz, passband return loss of 25 dB at static state and center frequency tunable range between 1.60 GHz and 2 GHz. Fig. 9(a) shows the physical layout with dimensions. The modulation parameters are selected by using (7) and (8). The optimization of the physical dimensions of the proposed NBPFs are carried out using ANSYS HFSS and

Table 3
Performance comparison proposed non-reciprocal bandpass filters with previously published works.

	Technology	Z_s/Z_L (Ω)	Frequency tunability range: FTR (GHz)	IL_{max} (dB)	RL_{min} (dB)	IX @f_0 (dB)	$BW_{3\text{-}dB}$ (MHz)	BW_{IX} (MHz)	$BW_{16\text{-}dB\text{-}IX}$ (MHz)
[23]	Lumped	50-to-50	0.136–0.163 (18.06 %)	3.70–4.10	>14	9–52.8	27.5	4	6
[24]	Lumped	50-to-50	0.270–0.310 (13.79 %)	1.7–4.30	>10	15.4–30.9	25	3	6
[27]	Lumped	50-to-50	0.190	1.50	>15	20	33	15	23
[28]	Lumped	50-to-50	0.150	1.5	>17	15	120	10	14
[29]	Microstrip	50-to-50	0.96	4.50	>10	18.3	57	NA	25
[30]	Microstrip	50-to-50	1.02	2.70	>12	11.7	65	NA	NA
[31]	Microstrip	50-to-50	0.885–1.031 (15.24 %)	2.2–2.80	>16.1	23.2	96	42	52
[32]	Microstrip	50-to-50 (25 + j10)-to-50 (25 + j10)-to-(55 + j10)	1.64–1.97 (18.28 %) 1.65–1.97 (17.67 %) 1.66–1.97 (17.08 %)	3.94–4.92 3.96–4.98 3.98–5.01	>11	20.78–23.55 22.02–23.45 20.59–21.48	85–90	52	65
[33]	Microstrip	50-to-50	1.45–1.55 (6.670 %)	3.40–3.71	>10	10	NA	NA	NA
[34]	Microstrip	50-to-50	1.08	3.60	>12	36.2	130	10	15
[35]	Microstrip	50-to-50	1.65–1.95	3.2–4.82	>12	22.1–34.5	102–115	10	15
[36]	Microstrip	50-to-50	0.725*	3.20	>15	6.8–62.1	90	5	10
[37]	Microstrip	50-to-50	1.46	3.10	>15.2	20.2	130	50	60
This work	Microstrip	50-to-50 (27 + j12)-to-50 (25 + j12)-to-(55-j5)	1.62–1.94 (17.98 %) 1.62–1.94 (17.98 %) 1.62–1.92 (16.94 %)	4.30–5.40 4.32–5.46 4.47–5.58	>12 >11.5 >13.3	22.90–24.24 22.07–33.87 22.30–31.25	106–124 109–124 110–126	>125 >130 >110	AFR (∞) AFR (∞) AFR (∞)

IL_{max}: Minimum in-band insertion loss, RL_{min}: Input and output in-band return loss, Z_s: port 1 termination impedance, Z_L: port 2 termination impedance.
BW_{3dB}: Forward transmission 3-dB bandwidth, BW_{IX}: 20-dB reverse isolation bandwidth within passband.
$BW_{16\text{-}dB\text{-}IX}$: 16-dB reverse isolation bandwidth, AFR: all frequency range, *: Differential non-reciprocal bandpass filter.

Keysight ADS co-junction with HB module. In this work, we used varactor diode SMV 1233-079LF which provides capacitance range of 1–20 pF under reverse bias voltage range of 15–0 V [39]. The progressive phase shift sinusoidal signals are applied using Keysight signal generator whereas the measured *S*-parameter results are obtained using Keysight N5224A vector network analyzer.

3.1. Results of prototype 1: Filter A: 50-to-50 Ω NBPF

The physical dimensions of NBPF with RF port 1 and port 2 termination impedances of 50 Ω (Filter A: 50-to-50 Ω) are illustrated in Fig. 9 (a). The photograph of fabricated filter is depicted in Fig. 9(b). Fig. 10(a) depicts the simulated and measured frequency response of Filter A at center frequency of 1.74 GHz. The measured frequency response closely matches with the simulated results and a summary of the measured results can be found in Table 2. In experimental results, the minimum measured in-band IL ($|S_{21}|$) is 4.72 dB while maintaining in-band input and output RLs higher than 13.4 within 3-dB passband bandwidth of 112 MHz. The reverse IX remains higher than 20 dB across the entire frequency range.

Fig. 11(a) depicts both the simulated and measured *S*-parameters of Filter A, illustrating the frequency tunability response. While Fig. 11(a) shows a finite number of frequency responses, it is important to note the passband center frequency can be continuously adjusted from 1.62 to 1.94 GHz by tuning dc-bias voltage of 0 to 5.20 V, while maintaining in-band return loss >12 dB and IX >16 dB for entire frequency range. The in-band IL loss varied from 4.30 dB to 5.40 dB throughout the entire tuning range of 1.92 GHz to 1.62 GHz. The IL is primarily attributed because of parasitic resistance of varactor diode. When a center frequency is tuned toward a lower value, the IL slightly increases. The increase in parasitic resistance of varactor diode is mainly responsible for deterioration in IL and this effect becomes more prominent as the dc-bias voltage is decreased toward lower value. As shown in the figure, transmission zeros are produced in the forward direction of transmission due to cross-coupling resulting from progressive phase shift modulation signal. When resonators undergo modulation with progressive phase shift modulation signal, IM products are generated. Consequently, the power of RF signal is distributed among IM products, and transversal propagation of RF energy occurs not only through fundament frequency, but also through nonadjacent resonators at harmonic frequencies. This phenomenon leads to the generation of transmission zeros.

3.2. Results of prototype 2: Filter B: (27 + j12)-to-50 Ω NBPF

The physical dimensions of prototype 2 (Filter B: (27 + j12)-to-50 Ω) with port 1 impedance of (27 + j12) Ω and port 2 impedance of 50 Ω, are depicted in Fig. 9(a). Fig. 10(b) depicts frequency response of Filter B at center frequency of 1.76 GHz, while Fig. 11(b) depicts the simulated and measured frequency tunability response. The measurement results of Filter B are shown in Table 2. As shown in Fig. 10(b) and Fig. 11(b), the measured S-parameters are agreed well with simulations.

As observed in Fig. 11(b), the center frequency can be adjusted continuously from 1.62 GHz to 1.94 GHz by changing dc-bias voltage from 0 to 5.20 V, providing 3-dB bandwidth variation from 109 MHz to 124 MHz. For each center frequency tuning state, the measured in-band IL ($|S_{21}|$) varies from 4.32 dB to 5.46 dB while the reverse IX varied ($|S_{12}|$) is varied from 20.44 dB to 33.87 dB at center frequency. The reverse IX exceeded 20 dB within the passband and remained higher than 16.40 dB across the entire frequency range. Although RF port impedances port 1 and port 2 are arbitrarily terminated ($Z_s \neq Z_L \neq 50$ Ω), Filter B exhibits good impedance matching within passband, resulting the in-band input/output RLs higher than 11.20 dB. The photograph of Filter B is shown in Fig. 10(d).

3.3. Results of prototype 3: Filter C: (25 + j12)-to-(55-j5) Ω NBPF

The objective of the third prototype (Filter C) is to design a NBPF with termination impedance of (25 + j10) Ω at port 1 and (55-j5) Ω at port 2. The physical dimensions of Filter C are depicted in Fig. 9(a). Fig. 10(c) illustrates the simulated and measured *S*-parameter results of Filter C at center frequency of 1.76 GHz while Fig. 11(c) showcases the simulated and measured frequency tunability responses. The measured frequency response closely agrees with the simulations and summary of measured results of Filter C can be depicted in Table II. As shown in Fig. 11(c), the center frequency can be continuously tuned from 1.62 GHz to 1.94 GHz with 3-dB bandwidth variation from 110 MHz to 126 MHz. In each center frequency tuning state, the measured in-band IL ranged from 4.47 dB to 5.58 d, while the reverse IX varied from 20 dB to

30 dB at f_0. The reverse IX remains higher than 20 dB within the passband and exceeds 17.50 dB across the entire frequency range.

3.4. Discussion

The forward transmission IL of the proposed NBPF primarily results from two factors: (a) the conversion of a fraction of spectral RF power into intermodulation (IM) products and (b) presence of the parasitic resistance (R_s) in varactor diode. To explore the underlying cause of the forward transmission IL, we have conducted the simulation of NBPF using SPICE model of varactor diode SMV 1233-079LF. These findings indicate that a fraction of RF power distributed among IM products contributes to IL of 0.92 dB. The remaining IL is primarily attributed because of parasitic resistance R_s of the varactor diode. Notably, an increase in parasitic resistance (R_s) value correlated with higher forward transmission IL. To improve the IL, it is advisable to employ varactor diodes with small parasitic resistance (i.e. high Q-factor varactor diode).

The performance comparison between the proposed NBPFs and previously reported NBPFs are depicted in Table 3. Notably, the previously reported NBPFs [23,24,34–36] exhibit high reverse IX only at center frequency and reverse IX bandwidth is very narrow. Likewise, works [27–31,37] demonstrated NBPFs with two-null reverse IX characteristics. Although reverse isolation characteristics of these works have two nulls, reverse isolation bandwidths of 20-dB and 16-dB are very narrow and limited to range of 15–50 MHz and 23–65 MHz, respectively. In contrast, this work demonstrated NBPFs with center frequency tunability and arbitrary termination impedances that exhibited the high reverse IX over the wide bandwidth. The measured reverse IX is higher than 20 dB within passband and higher than 16.50 dB at entire frequency range.

4. Conclusion

In summary, this paper demonstrated rigorous design and microstrip line implementation of tunable non-reciprocal bandpass filters with arbitrarily terminated RF port impedances. The proposed non-reciprocal filter can achieve low forward transmission insertion loss, excellent impedance matching, and ultrawide high reverse isolation bandwidth. The accuracy of design has been confirmed through a comparison with the harmonic balance simulation results of microstrip line NBPF. For experimental validation, three prototypes of nonreciprocal bandpass filters have been designed, fabricated, and measured. The measured frequency responses of non-reciprocal bandpass filters are in good agreement with the simulated frequency responses, providing reverse isolation exceeding 18 dB at all frequency range. Moreover, the proposed filter successfully integrates matching circuit, tunable filter and ultrawide isolator functionalities into a single circuit.

Acknowledgments

This research was supported by National Research Foundation of Korea (NRF) grant funded by Korea Government (MSIT: Ministry of Science and ICT) (No. RS-2023-00209081), in part by the Basic Science Research Program through the NRF of Korea, funded by Ministry of Education (No. 2019R1A6A1A09031717).

References

[1] K. Park, J. Myeong, G.M. Rebeiz, B.W. Min, A 28-GHz full duplex phased array front-end using two-cross-polarized arrays and a canceller, IEEE Transactions on Microwave Theory Techn. 69 (1) (2021) 1127–1135.
[2] S. Hong, J. Brand, J. Choi, M. Jain, J. Mehlman, S. Katti, P. Levis, Application of self-interference cancellation in 5G and beyond, IEEE Communication Mag. 14 (2014) 114–121.
[3] N. Reiskarimian, J. Diakonikolas, T. Dinc, T. Chen, G. Zussman, H. Krishnaswamy, Integrated full duplex radios, IEEE Communication Mag. 55 (4) (2017) 142–151.
[4] N. Reiskarimian, A. Nagulu, T. Dinc, H. Krishnaswamy, Nonreciprocal electronic devices: a hypothesis tuned into reality, IEEE Microwave Mag. 20 (4) (2019) 94–111.
[5] Reines IC and Rebeiz GM. A robust high power-handling (> 10 W) RF MEMS switched capacitor. Proc. IEEE 24th Int. Conf. Micro Electro Mech. Syst., Cancun, Mexico. 2011. 764–767.
[6] C.E. Fay, R.L. Comstock, Operation of the ferrite junction circulator, IEEE Transactions on Microwave Theory Techn. 13 (1) (1965) 15–27.
[7] C.K. Seewald, J.R. Bray, Ferrite-filled anti-symmetrically biased rectangular waveguide isolator using magnetostatic surface wave modes, IEEE Transactions on Microwave Theory Techn. 58 (6) (2010) 1493–1501.
[8] H. Dong, J.R. Smith, J.L. Young, A wide-band, high isolation UHF lumped-element ferrite circulator, IEEE Microwave Wireless Compon. Lett. 2 (6) (2013) 294–296.
[9] A. Ashley, D. Psychogiou, Ferrite-based multiport circulators with RF co-designed bandpass filtering, IEEE Transactions on Microwave Theory Techn. 71 (6) (2023) 2594–2605.
[10] S. Tanaka, N. Shimomura, K. Ohtake, Active circulators: the realization of circulators using transistors, Proc. IEEE 53 (3) (1965) 260–267.
[11] T. Kodera, D.L. Sounas, C. Caloz, Magnetless nonreciprocal metamaterial (MNM) technology: application to microwave components, IEEE Transactions on Microwave Theory Techn. 61 (3) (2013) 1030–1042.
[12] C. Caloz, A. Alù, S. Tretyakov, D. Sounas, K. Achouri, Z.L. Deck-Léger, Electromagnetic nonreciprocity, Phys. Rev. Appl. 10 (4) (2018) 047001.
[13] A. Ashley, D. Psychogiou, On-chip GaAs-based dual-band bandpass filters/isolators (DBPFIs, Electronics Letter 59 (10) (2023) 1–3.
[14] D. Simpson, D. Psychogiou, MMIC active bandpass filter with nonreciprocal and quasi-elliptic response, IEEE Microwave Wireless Tech. 33 (2) (2023) 141–144.
[15] N. Reiskarimian, H. Krishnaswamy, Magnetic-free non-reciprocity based on staggered commutation, Nature Communication 7 (11217) (2016) 1–10.
[16] T. Dinc, M. Tymchenko, A. Nagulu, D. Sounas, A. Alu, H. Krishnaswamy, Synchronized conductivity modulation to realize broadband lossless magnetic-free non-reciprocity, Nature Communication 8 (795) (2017) 1–9.
[17] A. Nagulu, T. Dinc, Z. Xiao, M. Tymchenko, D. Sounas, A. Alu, H. Krishnaswamy, Nonreciprocal components based on switched transmission lines, IEEE Transactions on Microwave Theory Techn. 66 (11) (2018) 4706–4725.
[18] Y. Yu, G. Michetti, M. Pirro, A. Kord, D.L. Sounas, Z. Xiao, C. Cassella, A. Alu, M. Rinaldi, Radio frequency magnet-free circulators based on spatiotemporal modulation of surface acoustic wave filters, IEEE Transactions Microwave Theory Tech. 67 (12) (2019) 4773–4782.
[19] A. Kord, D.L. Sounas, A. Alu, Pseudo-linear time-invariant magnetless circulators based on differential spatiotemporal modulation of resonant junctions, IEEE Transactions on Microwave Theory Techn. 66 (6) (2018) 2731–2745.
[20] Kord A, Sounas DL, and Alu A. Differential magnetless circulator using modulated bandstop filters. In: IEEE International Microwave Symp. Dig. 2017. 384–388.
[21] N.A. Estep, D.L. Sounas, A. Alù, Magnetless microwave circulators based on spatiotemporally modulated rings of coupled resonators, IEEE Transactions on Microwave Theory Techn. 64 (2) (2016) 502–518.
[22] A. Kord, D.L. Sounas, Z. Xiao, A. Alu, Broadband cyclic- symmetric magnetless circulators and theoretical bounds on their bandwidth, IEEE Transactions on Microwave Theory Techn. 66 (12) (2018) 5472–5481.
[23] D. Simpson, D. Psychogiou, Magnet-less non-reciprocal bandpass filters with tunable center frequency, Proc. European Microwave Conf (2019) 460–463.
[24] D. Simpson, D. Psychogiou, Fully-reconfigurable non-reciprocal bandpass filters, IEEE International Microwave Symposium Dig. (2020).
[25] G. Chaudhary, Y. Jeong, Unequal power division ration nonreciprocal filtering power divider with arbitrary termination impedance and center frequency tunability, IEEE Trans. Microw. Theory Techn. (2023). Early access.
[26] J. Zang, S. Wang, A. Alvarez-Melcon, J.S. Gomez-Diaz, Nonreciprocal filtering power dividers, Int. J. Electron. Commun. (AEU) 132 (2021) 153609.
[27] X. Wu, X. Liu, M.D. Hickle, D. Peroulis, J.S. Gomez-Diaz, A. Alvarez-Melcon, Isolating bandpass filters using time-modulated resonators, IEEE Transactions on Microwave Theory Techn. 67 (6) (2019) 2331–2345.
[28] P. Dutta, G.A. Kumar, G. Ram, Numerical design of non-reciprocal bandpass filters with the aid of 3D coupling matrix for 5G bands. IEEE trans. circuits and systems-II, express, Briefs 69 (7) (2022) 3334–3338.
[29] A. Alvarez-Melcon, X. Wu, J. Zang, X. Liu, J.S. Gomez-Dıaz, Coupling matrix representation of nonreciprocal filters based on time modulated resonators, IEEE Transactions on Microwave Theory Techn. 67 (12) (2019) 4751–4763.
[30] Wu X, Nafe M, Alvarez Melcon A, Gomez-Dıaz JS, and Liu X. A non-reciprocal microstrip bandpass filter based on spatio-temporal modulation. in 2019 IEEE International Microwave Sympo. (IMS). 2019. 9–12.
[31] X. Wu, M. Nafe, A. Alvarez Melcon, J.S. Gomez-Dıaz, X. Liu, Frequency tunable non-reciprocal bandpass filter using time-modulated microstrip $\lambda_g/2$ resonators. IEEE trans. circuits and systems-II: express, Briefs 68 (2) (2021) 667–671.
[32] G. Chaudhary, Y. Jeong, Frequency tunable impedance matching nonreciprocal bandpass filter using time-modulated quarter-wave resonators, IEEE Transactions on Industrial Electronics 69 (8) (2022) 8356–8365.
[33] Chaudhary G, Lee J, Pech P, and Jeong Y. Microstrip line non-reciprocal bandpass filter with tunable center frequency. Proc. IEEE International Symposium on Radio-Frequency Integrated Technology (RFIT). 2022. 188-190.
[34] D. Chatzichristodoulou, S. Arain, C. Pavlou, L. Vassiliou, D. Psychogiou, S. Nikolaou, P. Vryonides, Spatiotemporal modulated three-pole nonreciprocal quasi-elliptic bandpass filter, Proc. European Microwave Conference (2022) 289–292.
[35] G. Chaudhary, Y. Jeong, Non-magnetic non-reciprocal bandpass filter with quasi-elliptic response and tunable center frequency, AEU International Journal of

Electronics and Communications 175 (2024) 155111, https://doi.org/10.1016/j.aeue.2023.155111.
[36] D. Simpson, P. Vryonides, S. Nikolaou, D. Psychogiou, Non-reciprocal balanced bandpass filters with quasi-elliptic response. IEEE trans. circuits and systems-II: express, Briefs 69 (12) (2022) 5159–5162.
[37] G. Chaudhary, Y. Jeong, Nonreciprocal bandpass filter using mixed static and time-modulated resonators, IEEE Microwave Wireless Components Letters 32 (4) (2022) 297–300.
[38] R.J. Cameron, C.M. Kudsia, R. Mansour, Microwave filters for communication systems: fundamentals, design and applications, New York, NY, Wiley, USA, 2007.
[39] SMV123x series: Hyper abrupt junction tuning varactors, Skyworks Solutions, Inc.